Journal of Photochemistry and Photobiology A: Chemistry 211 (2010) 59–64

Contents lists available at ScienceDirect

Journal of Photochemistry and Photobiology A: Chemistry

journal homepage: www.elsevier.com/locate/jphotochem

SEM and Raman study of thermally treated TiO_2 anatase nanopowders: Influence of calcination on photocatalytic activity

N. Mahdjoub, N. Allen*, P. Kelly, V. Vishnyakov

Dalton Research Institute, Manchester Metropolitan University, Manchester, M1 5GD, UK

ARTICLE INFO

Article history:
Received 12 November 2009
Received in revised form 14 January 2010
Accepted 8 February 2010
Available online 16 February 2010

Keywords:
Titanium dioxide
Photocatalysis
Calcination
Dye fading
Raman

ABSTRACT

Titania (TiO_2) nanopowders called PC 500, synthesised by the sulphate process, were annealed in air at temperatures of up to 1022 K for 30 min. The X-ray Diffraction (XRD) indicates that the thermal annealing resulted in coarsening of the average crystallite size from 13 to 72 nm. However, Scanning Electron Microscopy (SEM) reveals persistence of platelet-like structures which survive up to temperatures around 900 K. This implies that the crystals at least partially grow within the plates in 2D confinement. This implies that direct usage of Scherrer equation in this case should be approached with care. Raman spectra peak positions and the Full-Width-at-Half-Maximum (FWHM) values changed considerably after calcinations crystal growth, while, material composition and oxygen content remain unchanged. The Raman peak behaviour can be cautiously attributed to the first order phonon confinement phenomena, but both, 2D and 3D models of confinement should be accounted. The highest photoactivity, as indicated by photoinduced degradation of a mono azo dye methyl-orange ($C_{14}H_{14}N_3SO_3Na$), was observed in material treated at 773 K.

1. Introduction

Titania (TiO_2) is widely used in a variety of industrial applications and products, such as catalysis, charge separating devices, chemical sensors, solar cells, microelectronics, electrochemistry, foods and pharmaceuticals [1]. The high refractive index, durability and non-toxic nature of titania, together with its capability to reflect or scatter light, has led to its extensive use in paints, plastics, inks and paper as a white pigment [2]. Titania is also one of the most studied semiconductors for photocatalytic reactions due to its low cost, simplicity of handling and resistance to photoinduced decomposition. Titania exists in various crystalline phases, three of which—rutile, brookite, and anatase can be considered as most studied. The titanium ion coordinates with six oxygen atoms in each form. Anatase and rutile are tetragonal, while brookite is orthorhombic. Anatase and brookite are relatively thermodynamically unstable forms and transform at high calcination temperatures to rutile.

Due to its commercial importance, the synthesis and characterization of TiO_2 nanopowders has attracted much interest in the last few years, and have given rise to a diversity of preparation methods, which influence the morphology and size of the nanoparticles [1,3]. The morphology of a powder controls its ability to flow and blend with other particles and the crystallite size controls the specific surface area, which is important in catalysis. It is therefore important to study the morphology and characteristics of TiO_2 powders [4,5]. The anatase nanopowders used in the present study were synthesised by the sulphate process and are referred to as 'PC 500'. These powders have been annealed in air at temperatures up to 1022 K for 30 min. In this paper, we report on the changes in crystallite size due to this thermal treatment and the influence this treatment had on the micro-Raman spectra of the powders. Crystallite size estimates were made from broadening peaks, and these measurements were supported by low energy SEM analysis.

The photocatalytic activity of titania depends on crystal phase, particle size and degree of crystallinity. It is widely accepted that from the known crystalline forms of titania, anatase and anatase/rutile mixtures are the most active compositions, compared to the pure rutile and brookite phases. In terms of particle size, photocatalytic activity would also be expected to depend on surface to volume ratio. Consequently in order to correlate phase and crystallite size to the photocatalytic activity of titania, the photocatalytic oxidation of a mono azo methyl-orange (MeO) dye by titania nanopowder samples under UV irradiation has also been studied [6–9]. In the photodegradation of MeO, illumination of titania by photons of energy greater than the band gap energy creates pairs of electrons (e^-) and holes (h^+) following the reaction [10–13]:

$$TiO_2 + h\nu \rightarrow TiO_2(e^-, h^+)$$

The photogenerated holes migrate to the interface and react with OH^- adsorbed onto the TiO_2 to create hydroxyl radicals (•OH):

* Corresponding author. Tel.: +44 01612471432.
E-mail address: n.S.allen@mmu.ac.uk (N. Allen).

1010-6030/$ – see front matter © 2010 Elsevier B.V. All rights reserved.
doi:10.1016/j.jphotochem.2010.02.002

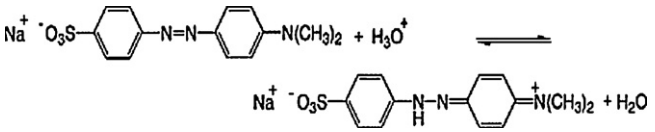

Fig. 1. Structure formula of methyl-orange.

$$(TiO_2)\cdots OH^- + h^+ \rightarrow {}^{\bullet}OH$$

The $^{\bullet}OH$ radicals have extremely strong oxidising properties and are able to decompose MeO dye. The probability to decompose is then linked to efficiency of hole generation, hole mobility, transport phenomena and, ultimately, crystalline size The paper aims to investigate of effects of thermal annealing (calcinations) on manifestation of crystalline structure and variation of photocatalytical activity.

2. Experimental

2.1. Titania nanopowder preparation

The samples analysed in this work were prepared by the sulphate process and were provided by a private company, consequently detailed of synthesis and selection were not provided.

2.2. Material characterization

The titania samples were characterised by XRD, SEM and micro-Raman spectroscopy. Nano-crystallite sizes were estimated from XRD spectra by use of Scherrer's equation:

$$D = \frac{k\lambda}{\beta \cos\theta}$$

where D is the grain size; k is a constant (shape factor), λ is the X-ray wavelength, β is the Full-Width-at-Half-Maximum (FWHM) of a characteristic diffraction peak and θ is the diffraction angle.

Micro-Raman analysis was carried out using an Invia-Microscope from Renishaw with a micro-Raman spot size of 0.8 μm. Spectra were taken from each sample in 5–6 places and the results were averaged. The spectra were taken at room temperature with a 514 nm Argon laser. SEM micrographs were taken at room temperature with a Field Emission Gun (FEG) Zeiss Supra 40VP system. The images were made at short working distance (3 mm) with a small spot size (1.2 nm) in order to obtain better resolution.

2.3. Reagents and photocatalysis mechanism

The measurements of photocatalytic activity were based on the degradation of the methyl-orange (MeO) reagent. Methyl-orange (MeO) analytical grade (99.9%) purity) from Aesar Alfa was used as a simple model of a series of common azo dyes largely used in the industry. This material is known as an acid–base indicator, orange in basic medium and red in acidic medium. Its structure is characterised by sulphonic acid groups, known to be responsible for the high solubility of these dyes in water is presented Fig. 1.

When it is dissolved in distilled water, the MeO UV–vis spectrum showed two absorption maxima (see for example Fig. 6). The first band is observed at approximately 270 nm and the second, much more intense band is observed at approximately 458 nm. Changes in these reference bands were used to monitor the photocatalytic degradation of MeO by the nanopowders catalysts. Experiments were carried out at room temperature in a static batch photo reactor consisting of a pyrex cylindrical flask open to air. The use of a magnetic stirrer ensured oxygenation from atmospheric air and a satisfactory mixing of the solution with the nanopowders. The irradiation of the mixture was performed by using artificial UV–vis polychromatic light source emitting at a wavelength of 365 nm with an intensity of 0.6 W/m^2 (the instrument used was a "Rank Aldis Tutor 2").

0.1 L of the reacting mixture was prepared by adding 0.3 g of TiO_2 catalysts into distilled water containing some amount (1 mL) of MeO (0.06 M). The mixture was stirred and irradiated for 3 h; samples of 5 mL were then withdrawn from the reactor every 30 min and separated from the TiO_2 particles using filtering syringe. The MeO removal of the dye solution was determined by measuring the absorbance value at 458 nm, using a UV–vis spectrophotometer calibrated in accordance with the Beer–Lambert's law.

Table 1
XRD Crystallite size of the powder at different calcinations temperatures.

PC 500	Calcinations temperature (K)	XRD crystallite size (nm)
	As synthesised	Non-determined (ND)
PC 500_572 K	572	13
PC 500_672 K	672	ND
PC 500_772 K	772	20
PC 500_872 K	872	26
PC 500_972 K	972	43
PC 500_1022 K	1022	72

3. Results and discussion

3.1. Size determination from XRD and SEM

X-ray Diffraction (XRD) spectra taken in 2θ configuration have exhibited peaks characteristic of the anatase phase. The averaged anatase grain sizes were determined using Scherrer's equation. The estimated crystallite sizes are listed in Table 1 and are shown in Fig. 2.

From this data it is possible to see that the crystallite size increases consistently with the temperature of calcination, from 13 nm as synthesised powder up to 72 nm at 1022 K (values were determined by a private company).

Selected SEM images of some of the thermally treated anatase powders are shown Fig. 3; PC 500 at room temperature, powder A treated at 297 K, 597 K, 897 K and 1022 K. For all but the highest cal-

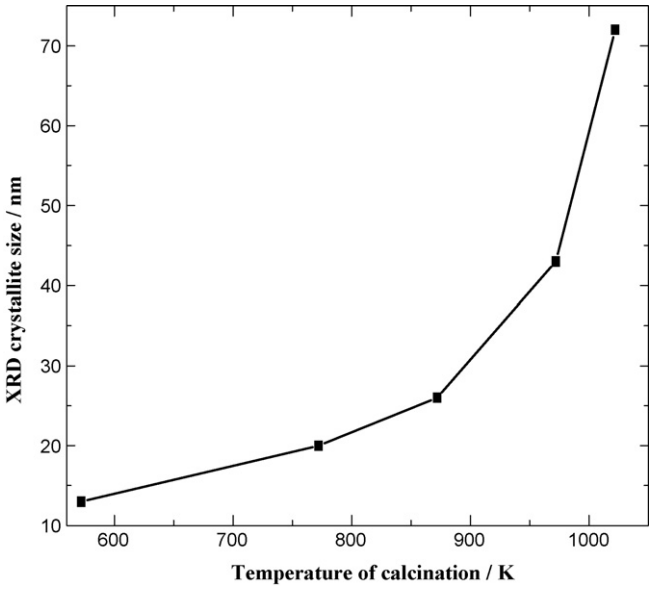

Fig. 2. XRD crystallite size/nm against the temperature of calcinations/K.

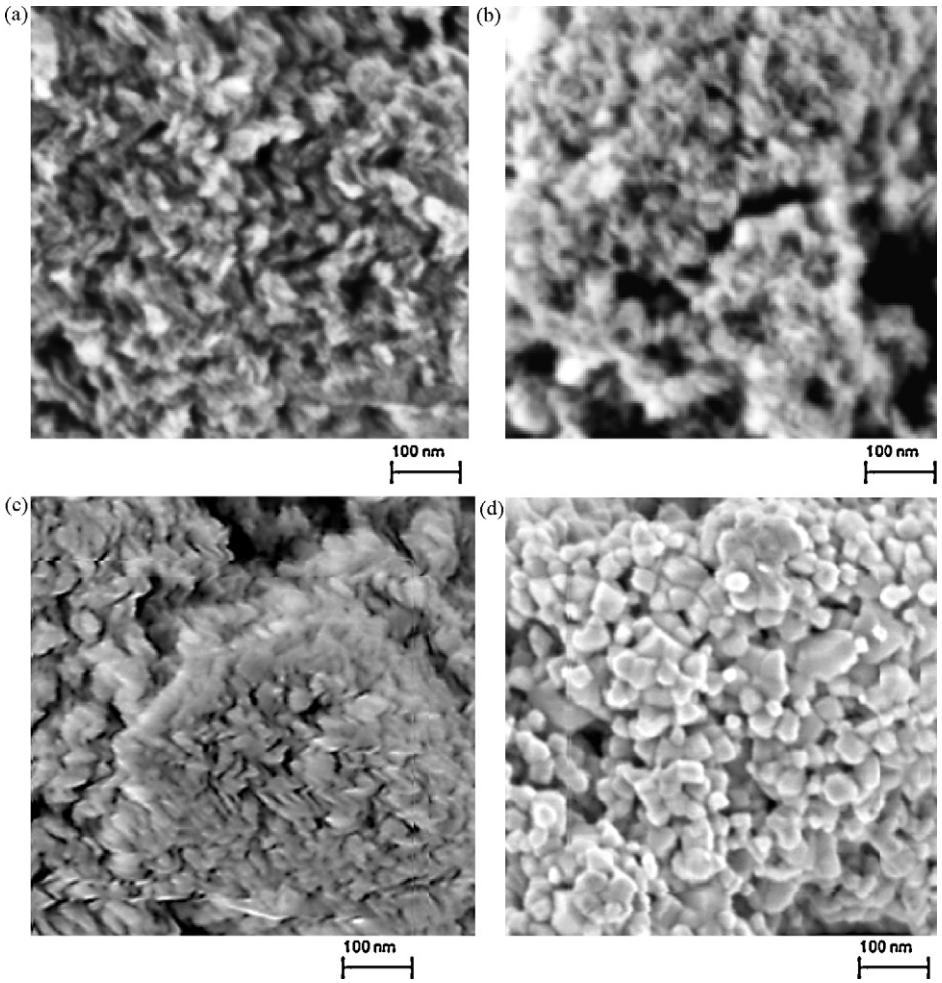

Fig. 3. SEM images of TiO_2 PC 500 powders thermal treated in air at; (a) as-prepared room temperature 297 K, (b) 597 K, (c) 897 K and (d) 1022 K.

cination temperature the images show what appears to be rather larger particles than those suggested by direct usage of Scherrer equation particles. It is possible that some particles are in an amorphous form. More detailed image analysis also suggests that a significant portion of the particles appear to be in a platelet form, e.g. the particles have in one direction a size at around 10 nm, while two other dimensions are much larger and are at around 30–60 nm. This effect cannot be accounted by direct use of Shrerrer's equation. The platelet particles are still present after calcination at 972 K. Only after calcination at 1022 K does the powder structure change completely and the platelet particles vanish. Nevertheless, a combination of XRD results with SEM data allows us to speculate that the initial small crystallites are at least partially imbedded into the platelet structures and at calcination temperatures below 1022 K grow within the platelet. While two dimensions of the crystal in this case will be in excess of 40 nm at a temperature 972 K, the third dimension will be limited to a smaller 10 nm region.

3.2. Raman spectroscopy

The Raman spectra for all the samples reveal characteristic peaks that are broader and shifted with respect to those of a bulk anatase crystal [14]. Table 2 shows the peak positions (cm^{-1}) of the vibrational modes of pure anatase. Fig. 4 shows Raman spectra of PC 500 annealed at 572 K, 872 K and 1022 K.

The peak position and width were determined by spectral deconvolution. The peak width (FWHM) is drawn against calcination temperature and XRD crystallite size on Fig. 5. The observed

Table 2
Peak positions/cm-1 of the vibrational modes of pure anatase.

A_{1g}	B_{1g}	c	E_g
515(m)	399(s) 795(w)	320(vs)	144(vs) 197(w) 639(m)

vs, very strong; s, strong; m, medium; w, weak; sh, shoulder band; c, combination.

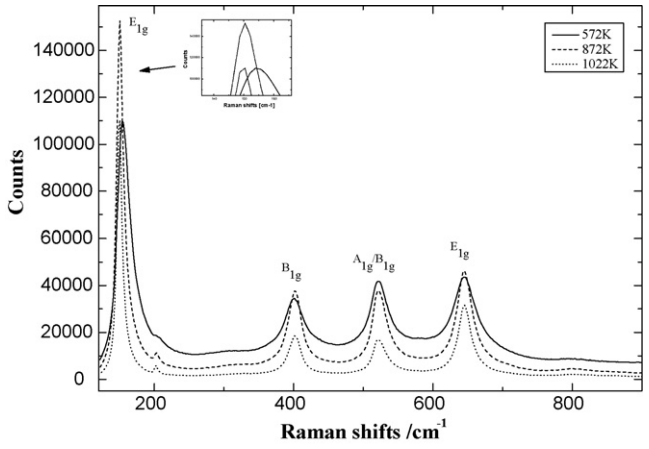

Fig. 4. Raman spectra of the PC 500 TiO_2 nanopowders; at 572 K (13 nm), at 872 K (26 nm), and at 1022 K (72 nm).

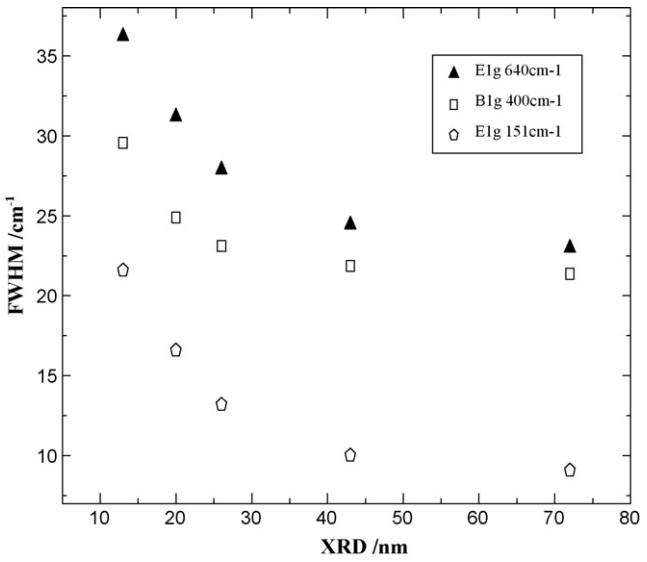

Fig. 5. FHWH/cm^{-1} of each peaks against XRD crystallite size/nm.

line broadening can be understood with the breakdown of the phonon momentum selection rule $q = 0$, characteristic of the Raman scattering in ordered systems. If the crystals are very small the selection rule is not valid anymore, since the phonons are confined and all the phonons over the Brillouin zone will contribute to first order Raman spectra. The weight of the "off-center" phonons increase as the crystals size decrease and the dispersion of the phonon involve an asymmetrical broadening and a shift of the Raman peaks. As expected from the confinement theory all peaks get narrower as the crystallite size increases [15,16]. There are two types of confinement model; the 3D and the 2D. According to the SEM images acquired, significant numbers of crystals are confined into platelets during initial stages of growth. It is most probable to have in this case a mixed asymmetrical confinement which could be assessed in some combined model by weighting the contributions of the 3D and 2D confinement model. However, at the moment there is not enough data to pursue this goal.

Concerning the peak positions, Fig. 6 shows the variation of position (cm^{-1}) with the crystallite size (nm^{-1}). For the lowest frequency mode E_{1g} (151 cm^{-1}), the peak shift to lower frequencies with calcination temperature and, therefore, the grain size increases. In contrast, the B_{1g} (396 cm^{-1}) peak shifts to higher frequency with increasing temperature and the second mode E_{1g} at 639 cm^{-1} does not seem to be significantly affected by temperature.

It has been shown in a previous study that anatase thermally treated in a purely N_2 environment is deficient in oxygen, although particles thermally treated in an oxidising environment maintain their stoichiometry [1]. Our samples were calcinated in air and should maintain their oxygen content. The sample composition was measured by Energy Dispersive X-ray analysis (EDX) and while the accuracy of the method in this case is at around 1%, no variation in oxygen content was found. On this basis it is believed that there is no measurable oxygen loss during calcination and all observed peak variation phenomena is purely attributed to crystal growth.

In summary, the low energy E_g peak shifts from 146 to 154 cm^{-1} after temperature treatment at 1022 K and the peak FWHM changes from 29 to 11 cm^{-1}. The low energy B_{1g} peak shows a blue shift from 396 to 397 cm^{-1} and changes FWHM from 31.5 to 22 cm^{-1}. The high energy E_g peak changes position from 641 to 638.5 cm^{-1} and FWHM from 35 to 22 cm^{-1}. The broadening and shifts of the Raman line shapes can be explained by the phonon confinement model [16–17].

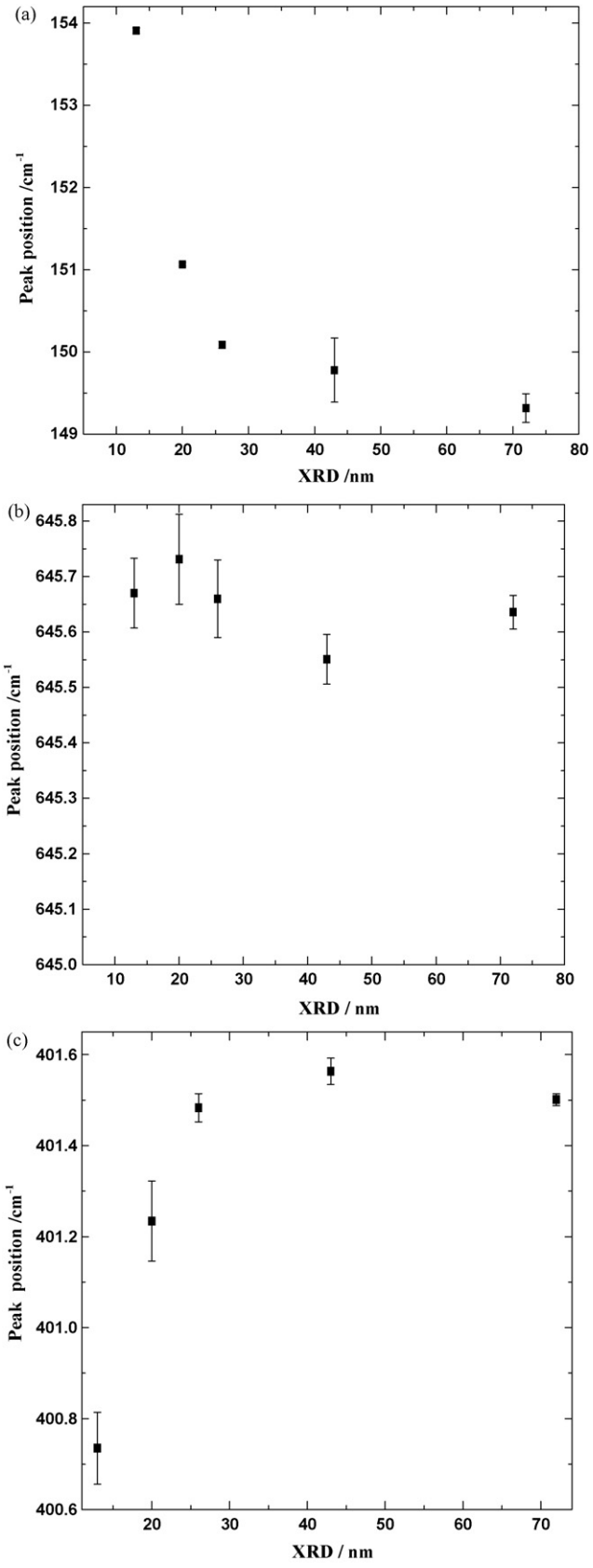

Fig. 6. Peaks position/cm^{-1} against XRD crystallite size/nm. (a) E_{1g} (151 cm^{-1}) peak position/cm^{-1} against XRD crystallite size/nm. (b) E_{1g} (639 cm^{-1}) peak position/cm^{-1} against XRD crystallite size/nm. (c) B_{1g} (396 cm^{-1}) peaks position/cm^{-1} against XRD crystallite size/nm.

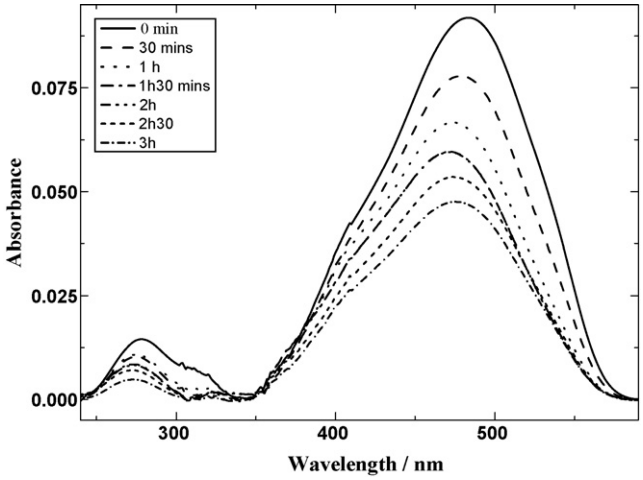

Fig. 7. Example of UV–vis spectra of MeO absorption for PC 500 nanopowders as-prepared (RT).

3.3. Photocatalytic activity

It is known that the colour of azo dyes such as MeO is determined by the azo bonds (–N=N–) and their associated chromophore and auxochromes. Decolouration of the dye indicates that it has been photochemically oxidised in a reaction. The MeO absorption shown in Fig. 7 highlights the phenomenon of degradation by the anatase nanopowders. As can be seen, the intensity of the peaks at 270 nm in the UV region and 480 nm in the visible region decrease progressively according to the time of irradiation.

Fig. 8 shows the normalised MeO concentration (%) as a function of irradiation time, for all investigated samples. It has been calculated by integrating the peak area of 472 nm diminishes. It can be seen that the powder activity significantly varies during calcination. Relatively high initial activity drops to low values at low annealing temperatures just to come though the peak activity for the sample as-prepared (at RT).

Complicated dependence of material activity on calcination temperature suggests that few different mechanisms are affected by the calcinations process. As was concluded earlier, low annealing temperatures lead to higher crystallinity in the powder. One can reasonably expect that the light absorption by the powder will decrease as the bandgap widens due to a reduction in absorption by the amorphous material. On the other side electrons and holes will have less scattering and recombination in a material with bigger crystallites. This will lead to a higher probability of excitations reaching the nanoparticle surface. On the other hand further crystal growth will inevitably reduce effective transportation to the surface and reduce surface-to-volume ratio, thus reducing photo activity. This description is speculative but probably is correct in general and more studies are needed to uncover particular mechanisms. The fact is that there is an optimum temperature which creates the most active nanopowder.

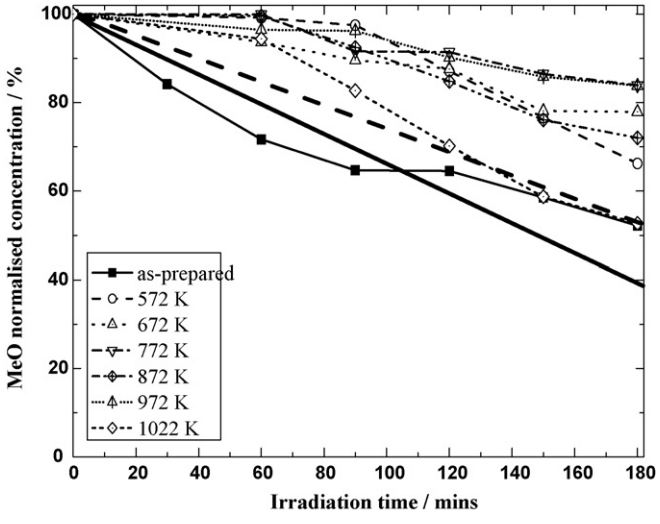

Fig. 8. Reduction of adsorption at 472 nm for solutions with nanopowders calcined at different temperatures/K.

4. Conclusion

Anatase TiO_2 nanopowders were synthesised by the sulphate process, and then annealed in air at temperatures up to 1022 K for 30 min. XRD study of nanopowders show that crystal size increases with annealing temperature. SEM revealed powder morphology and shows that some part of particles confined in platelet-like structures which is stable up to 972 K. Observed calcinations crystal coarsening is happening within platelets and is limited in one dimension by platelet thickness. Peaks in Raman Spectra get narrower as the result of calcinations and this can be described in broad terms on the basis of phonon confinement theory. However, the growth of crystals inside the platelets will require the combination of weighted combinations of 3D and 2D confinements in further studies The dependence of the size of the particles and the peak positions is even more complex and should be analysed with additional involvement of symmetry theory. The photocatalytic oxidation of a mono azo dye methyl-orange by the titania anatase nanopowders indicated that sample at its as-prepared conditions has the highest photocatalytic activity. The existence of peak activity can be understood on the basis of competing processes of efficiency of charge transportation to the surface and a relative reduction in the surface area due to the larger crystallites induced by the calcinations process.

References

[1] D. Bersani, G. Antonioli, P.P. Lottici, T. Lopez, Raman study of nanosized titania prepared by sol-gel route, Journal of Non-Crystalline Solids 232–234 (1998) 175–181.
[2] J.G. Balfour, Fine TiO_2, its properties and uses, Journal of New Matter 1 (1992).
[3] T. Ohsaka, F. Izumi, Y. Fujiki, Raman spectrum of anatase, TiO_2, Journal of Raman spectroscopy 7 (1978) 321–324.
[4] A. Amlouk, L. El Mir, S. Kraiem, S. Alaya, Elaboration and characterization of TiO_2 nanoparticles incorporated in SiO_2 host matrix, Journal of Physics and Chemistry of Solids 67 (2006) 1464–1468.
[5] N. Martin, C. Rousselot, D. Rondot, F. Palmino, R. Mercier, Microstructure modification of amorphous titanium oxide thin films during annealing treatment, Thin Solid films 300 (1997) 113–121.
[6] N. Guettaï, H. Ait Amar, Photocatalytic oxidation of methyl orange in presence of titanium dioxide in aqueous suspension. Part I: Parametric study, Desalination 185 (1–3) (2005) 427–437.
[7] L. Peruchon, L. Puzenat, E. Girard-Egrot, A. Blum, L. Herrmann, J.M. Guillard, Characterization of self-cleaning glasses using Langmuir–Blodgett technique to control thickness of stearic acid multilayers: importance of spectral emission to define standard test, Journal of Photochemistry and Photobiology A: Chemistry 197 (2–3) (2008) 170–176.
[8] Y. Badr, M.A. Mahmoud, Photocatalytic degradation of methyl orange by gold silver nano-core/silica nano-shell, Journal of Physics and Chemistry of Solids 68 (3) (2007) 413–419.
[9] A. Kontos, I. Arabatzis, I.M. Tsoukleris, D.S. Kontos, A.G. Bernard, M.C. Petrakis, D.E. Falaras, Efficient photocatalysts by hydrothermal treatment of TiO_2, Catalysis Today 101 (3–4) (2005) 275–281.
[10] S. Boujday, F. Wunsch, P. Portes, J.F. Bocquet, C. Colbeau-Justin, Photocatalytic and electronic properties of TiO_2 powders elaborated by sol-gel and supercritical drying, Solar Energy Materials and Solar Cells 83 (2004) 421–433.
[11] E. Alonso, I. Montequi, M.J. Cocero, Effect of synthesis conditions on photocatalytic activity of TiO_2 powders synthesized in supercritical CO_2, The Journal of Supercritical Fluids 49 (2) (2009) 233–238.

[12] A.L. Linsebieger, G. Lu, J.T. Yates Jr., Photocatalysis on TiO_2 surfaces: principles. Mechanisms, and selected results, Chemical Reviews 95 (1995) 735–758.
[13] W. Choi, A. Termin, M.R. Hoffmann, The role of metal ion dopenats in quantum-sized TiO_2; correlation between photoreactivity and charge carrier recombination Dynamics, Journal of Physics 51 (1994) 13669–13679.
[14] A. Li Bassi, D. Cattaneo, V. Russo, C.E. Bottani, Raman spectroscopy characterization of titania nanoparticles produced by flame pyrolysis: the influence of size and stoichiometry, Journal of Applied Physics 98 (2005).
[15] S. Balaji, Y. Djaoued, J. Robichaud, Phonon confinement studies in nanocrystalline anatase-TiO_2 thin films by micro Raman spectroscopy, Journal of Raman spectroscopy 37 (2006) 1416–1422.
[16] Ke-Rong Zhu, Ming-Sheng Zhang, Qiang Chen, Zhen Yin, Size and phonon-confinement effects on low-frequency Raman mode of anatase TiO_2 nanocrystal, Physics Letters A 340 (2005) 220–227.
[17] P.P. Lottici, D. Bersani, Applied Physics Letters 72/1 (1998) 73.